

PAPER • OPEN ACCESS

Ptychotomography at DLS Coherence Beamline I13

To cite this article: V.S.C. Kuppili *et al* 2017 *J. Phys.: Conf. Ser.* **849** 012031

View the [article online](#) for updates and enhancements.

Related content

- [The Wigner Function in Science and Technology: Quantum optics](#)
- [Coherence Length and Vibrations of the Coherence Beamline I13 at the Diamond Light Source](#)
- [A comparison of TEM and DLS methods to characterize size distribution of ceramic nanoparticles](#)

Recent citations

- [Materials characterization by synchrotron x-ray microprobes and nanoprobes](#)
Lorenzo Mino *et al*



IOP | ebooks™

Bringing together innovative digital publishing with leading authors from the global scientific community.

Start exploring the collection—download the first chapter of every title for free.

PTYCHOTOMOGRAPHY AT DLS COHERENCE BEAMLINE I13

V.S.C. Kuppili^{1,2}, S. Sala^{1,2}, S. Chalkidis^{1,2}, A.M. Wise⁶, A.D. Parsons³, I. Zanette³, C. Rau^{3,4,5}, P. Thibault²

¹Department of Physics and Astronomy, University College London, WC1E 6BT London, UK

²Department of Physics and Astronomy, University of Southampton, Southampton, SO17 1BJ, UK

³Diamond Light Source, OX11 0DE Didcot, UK

⁴School of Materials, University of Manchester, Grosvenor St., Manchester M1 7HS, UK

⁵Department of Otolaryngology, Northwestern University Feinberg School of Medicine, Chicago, Illinois 60611, USA

⁶SSRL, SLAC National Accelerator Laboratory, Menlo Park, CA 94025, USA

E-mail: ucapvsc@ucl.ac.uk

Abstract. We describe the implementation and execution of ptychotomography at I13-1, the coherence branchline at Diamond Light Source. The data collection and image reconstruction protocol is demonstrated with the three dimensional reconstruction of a nanoporous gold sample.

1. Introduction

Ptychography is a scanning coherent diffraction imaging technique in which the sample is scanned perpendicular to the path of X-ray beam, collecting diffraction patterns at each point. The points are chosen such that there is enough overlap of probe between adjacent points. The resulting far-field diffraction patterns are then processed through iterative phase retrieval algorithms to obtain high resolution, phase contrast transmission maps of an extended sample [1,2]. Usually phase contrast is significantly higher than absorption contrast in the hard X-ray regime [8]. A natural extension of two dimensional ptychographic imaging is the three dimensional analog, ptychotomography [3,4,7]. We exploit the high resolution 2D ptychographic projections obtained at various angles (figure 1) as a starting point which are then taken through the conventional tomographic process of alignment and 3D reconstruction thus obtaining a three-dimensional complex transmission map of the sample under study.



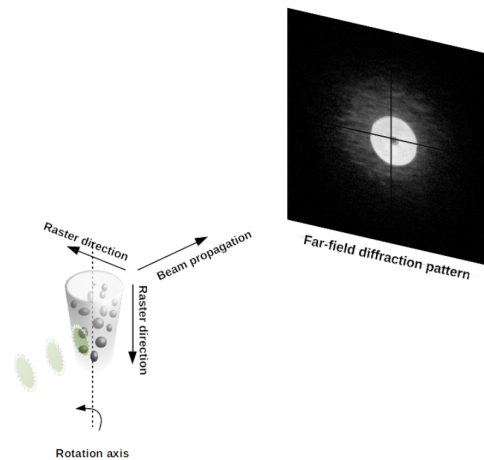


Figure 1. Schematic representation of the ptychotomographic experimental setup. The sample is rastered perpendicular to the X-ray beam collecting far-field diffraction patterns at each point. These patterns are taken through phase retrieval algorithms obtaining a ptychographic projection. Such projections collected at various angles constitutes a typical ptychotomographic dataset.

2. Experimental Details

3D nanoporous gold structures were prepared by selective dealloying of 33% gold-silver alloy micro whiskers (Palmer metals, UK). The micro whiskers were exposed to nitric acid (69% Sigma-aldrich) for 48 hours after which they were annealed for 18 hours at 375°C [5].

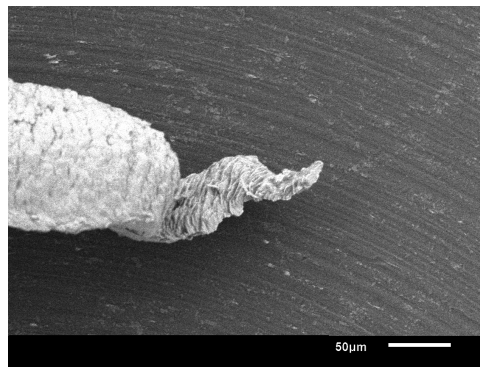


Figure 2. Scanning electron microscopy image of 33% gold-silver alloy micro whiskers dealloyed for 48 hours and then subjected to annealing for 18 hours at 375°C.

Ptychographic imaging was carried out at the I13-1, the coherence branchline of the I13 beamline at Diamond light source, UK [6]. The samples were imaged with X-rays at a photon energy 8.4keV and 0.1s exposure time per frame. The detector to sample distance was 6.7m. The photon counting Merlin detector with a pixel size of 55μm and 515x515 pixels wide was used. A zone plate, beam-stop, order sorting aperture ensemble was employed to obtain a confined (smaller than the field of view) X-ray probe in order to illuminate the sample. The reconstruction pixel size in this geometry was 35nm at the 512x512 cropping of the detector. 543 such equispaced angular projections were collected in interlaced format. The datasets were processed through

150 difference map iterations and 300 maximum likelihood iterations employing 3 probe modes for reconstruction (figure 3).

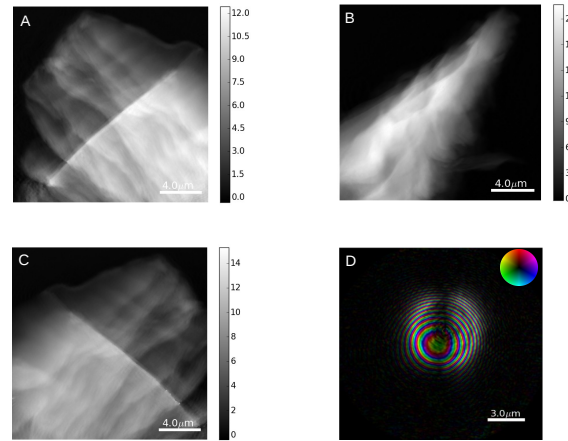


Figure 3. A,B,C. Phase unwrapped projections of nanoporous gold sample as seen in the figure 2 at 90, 0, 90 degrees respectively. The gray scale shows the phase shift in radians. D, is the primary mode of the orthogonalised probe. A colourwheel is used here to represent the complex-valued probe. The brightness of the pixel color corresponds to the magnitude of the probe while hue gives the relative phase of the probe.

In principle the raw ptychographic angular phase projections are corrected for phaseramp and phase unwrapped before taking them through the tomographic reconstruction routine. However presence of “residues”, points in phase that produce inconsistencies in phase unwrapping lead to imperfect unwrapping of phase in the angular projection. Imperfect phase unwrapping over the entire range of angular projections would result in overall blurring of the tomographic reconstruction. While phase unwrapping is necessary for alignment purposes, the 3D reconstruction itself can be obtained from phase wrapped angular projections. In order to get around this limitation, we have followed the approach suggested in [4] where a thinner portion of the projection which can be phase unwrapped easily is chosen as a representative element of the projection (figure 4). All further alignment routines are carried out with the representative elements and applied to the complete projection. The vertical alignment was done using edge detection method [3] and horizontal alignment was done using tomographic consistency technique [7].

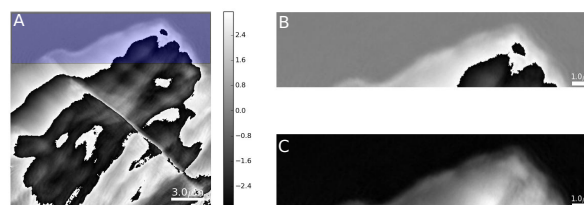


Figure 4. A, ptychographic projection after phase ramp removal. B, part of A used for alignment. C, same as B after phase unwrapping.

3. Results and Discussion

3D slices (figure 5) were then tomographically reconstructed by taking the derivatives of the aligned phase wrapped projections through the filtered back-projection technique [4]. We observe artefacts due to sharp edges (streak artefacts) and the fact that the sample is not completely in the field of view. Optimisation and standardisation of the ptychotomographic reconstruction routine is currently in progress.

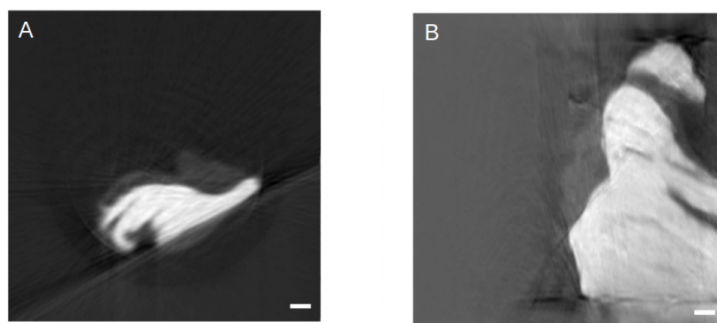


Figure 5. A, axial slice corresponding to 77th row of the phase projection. B, longitudinal slice. The scale bar in A and B corresponds to 1 micron.

4. Conclusions

We were successful in collecting and reconstructing three dimensional ptychotomographic data from the nanoporous gold sample, which is presently in the optimisation stage. The spatial resolution achievable with the current experimental setup is limited by the beam stability and the performance of the sample stages. Overheads mainly from the motor movements increase the data acquisition times and therefore (without any X-ray shutter) the risk of radiation damage is increased. We are currently in the process of achieving faster scan rates and making further improvements to the existing 3D data acquisition and reconstruction routines. We are heading towards execution and optimisation of multi-wavelength ptychographic imaging and on-the-fly scanning ptychotomography.

5. Acknowledgments

We acknowledge the financial support of ERC starting grant, OptimaX. We would like to thank Dr. Ulrich Wagner for facilitating the beamtimes at I13 coherence branch. We would like to thank Dr. Kaz Wanelik, Simon Logan, Andrew Wilson for their technical support. We thank Diamond Light Source for access to beamline I13-1 (MT13228) that contributed to the results presented here.

6. References

- [1] H. M. L. Faulkner and J. M. Rodenburg 2004 *Physical Review Letters* **93** 23901–23903
- [2] P. Thibault, M. Dierolf, A. Menzel, O. Bunk, C. David and F. Pfeiffer 2008 *Science* **379** 379–383
- [3] M. Dierolf, A. Menzel, P. Thibault, P. Schneider, C. M. Kewish, R. Wepf, O. Bunk and F. Pfeiffer 2010 *Nature* **467** 436–439
- [4] M. Guizar-Sicairos, A. Diaz, M. Holler, M. S Lucas, A. Menzel, R. A. Wepf and O. Bunk 2011 *Optics Express* **19** 21345
- [5] Y. Ding, Y. J. Kim and J. Erlebacher 2004 *Advanced Materials* **16** 1897–1900
- [6] Z. D. Pešić, A. D. Fanis, U. Wagner and C. Rau 2013 *Journal of Physics: Conference Series* **425** 182003
- [7] M. Guizar-Sicairos, J. Boon, K. Mader, A. Diaz, A. Menzel and O. Bunk 2015 *Optica* **2** 259–266
- [8] F. van der Veen and F. Pfeiffer 2004 *Journal of Physics: Condensed Matter* **16** 5003–5030